Molecular Packing in Crystalline Poly(9,9-di-*n*-octyl-2,7-fluorene)

S. H. Chen, H. L. Chou, and A. C. Su*

Institute of Materials Science and Engineering, National Sun Yat-sen University, Kaohsiung 804, Taiwan

S. A. Chen

Department of Chemical Engineering, National Tsing Hua University, Hsinchu 300, Taiwan

Received April 2, 2004; Revised Manuscript Received July 3, 2004

ABSTRACT: Presented are transmission electron microscopic observations of micron-sized single crystals of poly(9,9-di-*n*-octyl-2,7-fluorene) (PFO) prepared from thin films in the melt state. A preliminary determination of unit cell dimensions and molecular packing (orthorhombic, $a = 2.56$ nm, $b = 2.34$ nm, $c = 3.32$ nm, 8 chains, with space group $P2_12_12_1$ and density 1.041 g mL^{-1}) was made via combined considerations of the selected-area electron diffraction (SAED) pattern obtained along the [00*l*] zone of the single crystals, the SAED "fiber" pattern obtained from shear-oriented films, and the "powder" pattern from X-ray diffraction of melt-crystallized thick films in the absence of preferred orientation. In this model, PFO backbones are generally separated by transversely extended alkyl side chains, consistent with the dominance of single-chromophore emissions and the general lack of interbackbone delocalization of PFO chains in this ordered state as indicated by earlier photophysical studies. In addition, microscopic evidence for the presence of a vast number of nanograins was presented, and its implications in the crystallization process of semirigid PFO chains were discussed.

Introduction

Both poly(2-methoxy-5-(2′ethylhexyl)-1,4-phenylene-vinylene) (MEH-PPV) and poly(9,9-di-*n*-octyl-2,7-fluorene) (PFO, see inset of Figure 2c for chemical structure) have become the two representative light-emitting polymers that are subjected to extensive studies for elucidating the general photophysical nature of the light emission process and possible morphological effects involved.[1−3] It has been recently shown that MEH-PPV and its close homologues are typically mesomorphic, with only minor development of crystallinity.[4−7] In contrast, PFO is clearly crystalline with a melting temperature around 160 °C, above which a nematic (N) mesophase exists up to ca. 300 °C.[8−12] There may also exist a metastable β mesophase upon solvent vapor treatment or extensive thermal cycling in a subambient temperature range.[12−14] As these phases may be rather selectively maintained via proper selection of processing parameters (such as thermal history, solvent vapor treatment, and orientation in the nematic state by use of a rubbed polyimide substrate),[8,13,14] the resulting "morphological effects" in light-emission properties of PFO have been extensively examined in the literature.[15−18] However, the exact ways of molecular packing in these phases have remained obscure.[14,17] This renders earlier attempts to establish correlation between photophysical properties and morphological features imprecise.

In the pioneering X-ray diffraction (XRD) study of PFO by Grell et al.,[14] fiber patterns of the crystalline (α) phase (as well as those characteristic of mesomorphic β and N phases) have been obtained without further delineation of the crystal structure. This is understandably due to the apparent complexity of the fiber pattern as well as the lack of further evidence to narrow down the range of possible crystallographic choices. Here we present results of our recent transmission electron microscopic (TEM) observations over submicron-sized single crystals of PFO obtained via melt crystallization of thin films[19−21] cast on glass substrates. A combination of the selected-area electron diffraction (SAED) pattern along the [00*l*] zone as well as the "fiber" pattern obtained from shear-oriented specimens have thus allowed for preliminary determination of molecular packing in the α phase.

Methods

Experimental Details. The PFO sample used here was purchased from American Dye Source, Quebec, Canada (cat. no. ADS129BE). The weight-average molecular mass was 65 kDa and polydispersity index PDI = 2.6 as determined via GPC using polystyrene standards. Transmission electron microscopic (TEM) studies were performed using a JEOL 3010 instrument under an acceleration voltage of 200 kV, at which the combined factor of wavelength and camera length has been carefully calibrated using (111), (200), (220), and (311) reflections from vapor-deposited Al thin film. As the lifetime of selected-area electron diffraction patterns (SAED) of PFO single crystals in our specimens is generally less than 10 s under electron beam irradiation, special care was exercised via prefocusing at a neighboring region, repositioning of the specimen, followed by immediate taking of the SAED pattern. Relative intensities of the [00*l*] zonal spots were measured via combined use of MATLAB 6.1 and PhotoImpact 8 software, in which the intensity count for each spot was estimated by reading the peak height minus background. Surface topographic features were examined via secondary electron images (SEI) obtained by use of a field-emission scanning electron microscope (JEOL JSM-6330TF) under an accelerating voltage of 10 kV. Optical absorption (UV−vis) and photoluminescence (PL) spectra of the film specimens were obtained by use of a Hong-Ming MFS-230 instrument. A Bruker D8 Advance diffractometer equipped with a copper target (Kα line, with wavelength $\lambda = 0.154$ nm), a graphite collimator, and a vacuumed high-temperature stage (Anton Paar TTK-450) was used (under a step-scan rate of 0.05° per 3 s in the scattering angle range of $2\theta = 1°-41°$) to obtain "powder" X-ray diffraction (XRD) profiles of thick-film specimens in the absence of preferred orientation.

10.1021/ma049346a CCC: $27.50
Published on Web 08/11/2004

Specimens for TEM studies were cast from dilute (ca. 0.1% or lower) solutions of PFO in toluene on glass substrates. The as-cast films were then routinely vacuum-dried (in excess of 4 h at ca. 80 °C), melt-crystallized at an elevated temperature (typically in the range of 135−150 °C), followed by quenching in ice water and floating off the glass substrate using a dilute HF solution. In the case of oriented specimens, a manual shearing procedure (i.e., sweeping a blade over the melted thin film) was adopted prior to the heat-treatment step of melt crystallization. These specimens were then vapor-deposited with carbon or shadowed (with an incidence angle of 60° from plane normal) with a combined Pt/C source prior to TEM examinations. This procedure is in accordance with those[19−21] reported for semicrystalline polymers in general, except for slight modifications in minor details. Films for XRD studies were cast from more concentrated solutions (ca. 0.2% or slightly higher) for greater thickness and enhanced XRD signals.

Molecular Simulation. Molecular simulation studies were made on an O2 workstation equipped with the Cerius2 package (version 4.6, Accelrys). Among the five force fields built within Cerius2, the Universal force field[22] (UFF, version 1.02) was selected as it best reproduced experimental monomeric repeat length[4] for MEH-PPV (as a model polymer of conjugated backbone). A cutoff distance of 1.10 nm for nonbonded ver der Waals potentials was consistently adopted throughout the molecular simulation process. For visualization and presentation purposes, the WebLab ViewerPro (version 4.0, Molecular Simulations, Inc.) software was used.

The simulation procedure involved two stages. First, the single-chain conformation in a vacuum was determined via energy minimization of a PFO chain containing 50 repeating units. Chain conformation in the central section, presumably free of chain-end effects, was used as the "initial guess" of chain structure. This resulted in a perfect match of 0.83 nm in the length of repeating unit. The first-guess structure for the four repeat segments was then transposed to an orthorhombic unit cell with periodic boundary conditions and prescribed $P2_12_12_1$ space group, in which $c = 3.32$ nm (as dictated by XRD and SAED results) but $a = 25.6$ nm and $b = 23.4$ nm (i.e., 10 times that of the corresponding experimental values). The latter dimensions were then stepwise shortened (several percent in earlier steps but less than 1% in later steps) and energy-minimized under UFF in each step. This was continued until both *a*- and *b*-dimensions match the experimental values of $a = 2.56$ nm and $b = 2.34$ nm. Minor adjustments in the position and the azimuthal orientation of chains (as viewed along the *c*-axis) were then made manually (followed by further energy minimization under UFF) on a trial-and-error basis to fine-tune for optimal fit of the calculated to the experimental [00*l*] pattern. Dynamic effects in electron diffraction were not included in the calculations.

Results

Morphological Observations. In the case of single-crystal observations, carbon-coated specimens generally showed weak contrast in bright field images (BFI). The contrast was therefore enhanced via Pt shadowing. Representative BFI of melt-grown PFO single crystals on Pt-shadowed specimens are shown in Figure 1a,b with the corresponding SAED patterns as insets. Note that there exist a large number of nanocrystals on top of the sub-microsized single crystals; as these nanocrystals are rather thin and more or less randomly oriented, they contribute insignificantly to the [00*l*] zone patterns. Figure 1c shows a comparatively clear [00*l*] zone pattern that was obtained from a separate carbon-coated specimen without Pt shadowing (whose BFI contrast is low due to absence of shadows and hence not shown here; we emphasize here that this SAED pattern is in full agreement with the insets in Figure 1a,b although the latter are weaker in intensity). A representative BFI of shear-oriented specimen and the corresponding "fiber" pattern are shown in Figure 2a,b. Note that the latter is consistent with the XRD fiber patterns previously presented by Grell et al.[14]

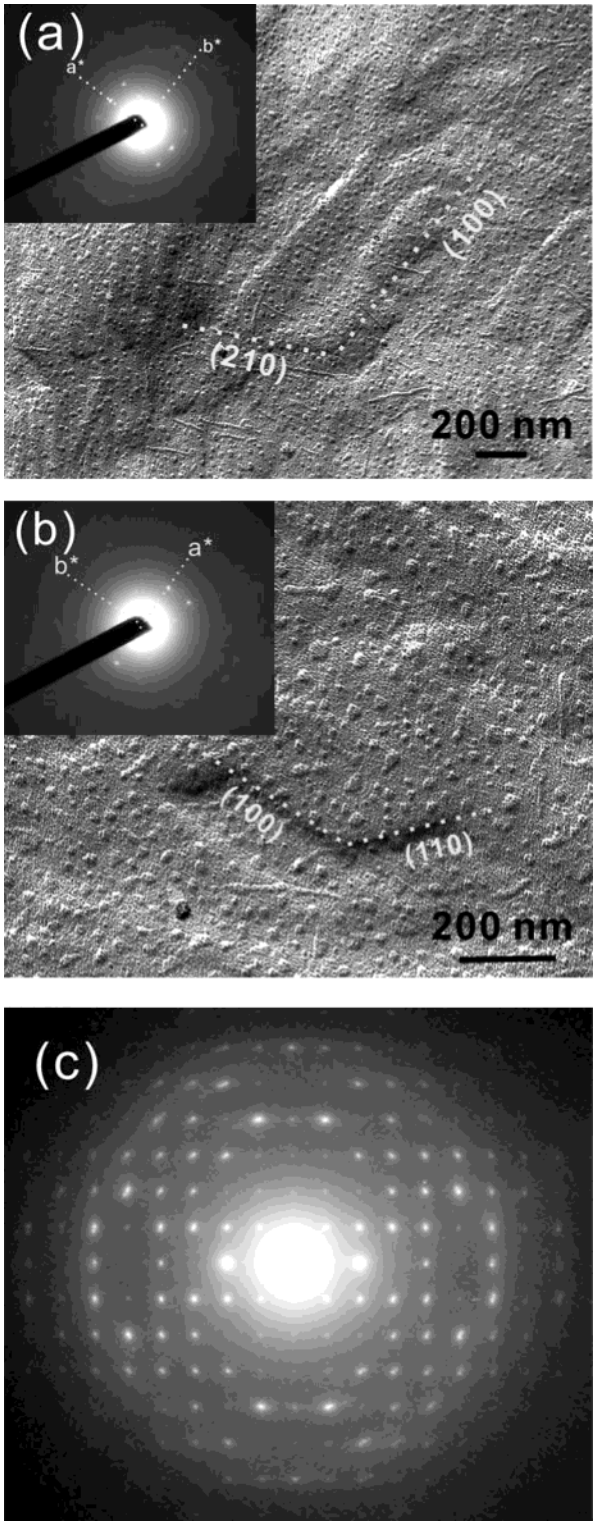

Figure 1. Representative bright field images and the corresponding SAED [00*l*] zone pattern of single crystals in PFO specimens heat-treated at 280 °C for 1 min and melt-crystallized at 148 °C for 12 h before quenching in ice water, showing (a) faceting along (100) and (210) planes and (b) more frequently observed faceting along (100) and (110) planes. Given in (c) is the clearest [00*l*] zone pattern obtained that was subsequently used in the structure determination for the α-phase.

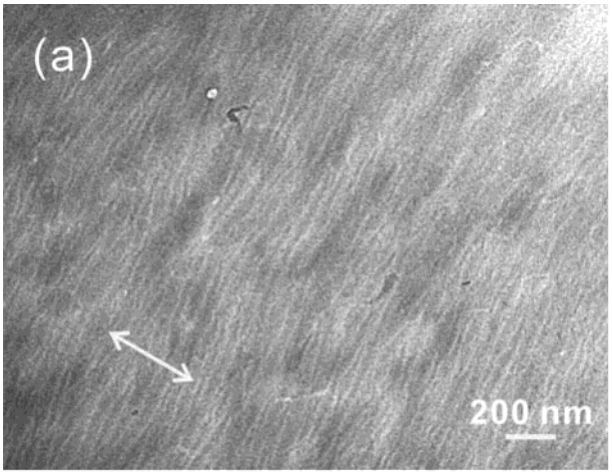

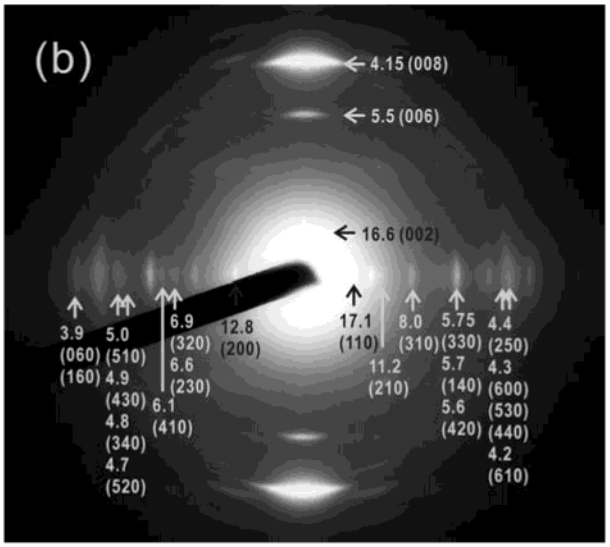

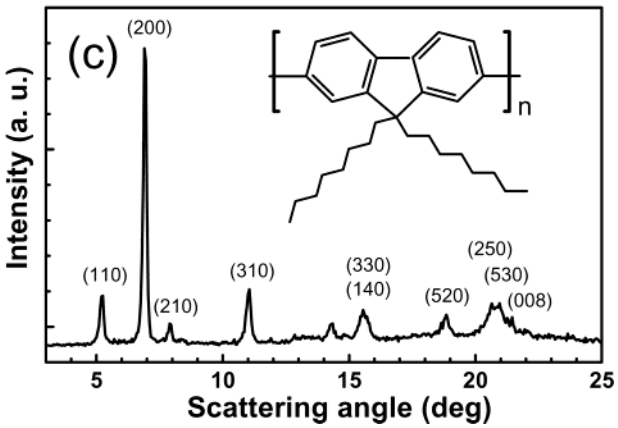

Figure 2. Representative (a) BFI and (b) SAED "fiber" pattern of PFO specimens shear oriented at 250 °C, followed by crystallization at 135 °C for 1 h before quenching in ice water; arrows in (a) and meridian in (b) correspond to the shear direction. The powder profile in (c) was obtained from a highly crystalline thick-film specimen after extended heat treatments at elevated temperatures and stepwise cooled to room temperature.

From Figure 1c, we have identified a total of 25 diffraction spots (including three meridional reflections) that are mirrored in the four quadrants defined along the two orthogonal reciprocal axes a^* and b^*. The diagram was indexed by a rectangular unit cell with dimensions $a = 2.56$ nm and $b = 2.34$ nm. Reflections

Table 1. Relative Intensities in the Experimental and Calculated [00*l*] Zone Patterns Shown in Figures 1c and 3d, Respectively

(*hkl*)	I_{obs}	I_{calc}	(*hkl*)	I_{obs}	I_{calc}
(020)	5		(410)	25	23
(110)	42	40	(060)	13	10
(200)	100	100	(330)	25	22
(120)	11	14	(420)	30	25
(210)	48	45	(600)	20	20
(040)	8	5	(160)	12	13
(130)	8	14	(250)	21	18
(220)	6	15	(430)	20	16
(310)	47	50	(520)	44	44
(400)	12	10	(610)	28	27
(140)	50	50	(440)	7	13
(230)	18	18	(530)	18	16
(320)	20	16	(620)	18	19

in the fiber pattern (Figure 2b) were then indexed and found to consistent with an orthorhombic unit cell where $c = 3.32$ nm along the fiber axis. The unit cell dimensions were consistent with the powder pattern given in Figure 2c. For the [00*l*] zone pattern, one may observe the systematic absence of odd reflections in (*h*00) and (0*k*0) series up to (700) and (070), respectively, whereas systematic absence of odd reflections in the (00*l*) series up to (009) is clearly identified in the fiber pattern. These observations indicate the presence of three 2-fold screws running along the *a*-, *b*-, and *c*-axes, respectively. We therefore assigned the space group as $P2_12_12_1$. Combined considerations over the symmetry operations involved, the length of the repeating unit (ca. 0.83 nm as given previously), and the plausibility of the derived density led us further to assume the presence of eight chains, each with four repeating units, in the unit cell; this gives a theoretical density value of 1.041 g/mL.

Molecular Packing. Energy-minimized packing of PFO chains via molecular simulation in the orthorhombic unit cell is shown in Figure 3a−c. The corresponding [00*l*] SAED zone pattern (cf. Figure 3d and Table 1) and powder XRD pattern (Figure 3e, simulated by assuming crystalline dimensions of 80 × 80 × 40 nm) calculated from this computer-generated structure reproduce rather well the main features of the experimental patterns shown in Figures 1c and 2c. A direct comparison between the simulated and experimental fiber patterns was not made, as many of the arcs in the latter (Figure 2b) overlap significantly with one another.

We note first that the fluorene repeat unit is *not* collinear: the inter-ring C−C bonds at both ends form an angle of ca. 160° (due to locking of the two phenylene rings by the bridgehead carbon at position 9), as first pointed out by Grell et al.[13] and confirmed in our molecular simulation. In addition, repulsion between the hydrogen atoms located at ortho positions of neighboring fluorene rings forbids strict coplanarity: neighboring fluorene units are typically twisted to form dihedral angles ranging from 15° to 24° (cf. Figure 3c). The lacking of both intramonomer collinearity and intermonomer coplanarity results in a low-symmetry backbone conformation, as reflected in the fact that four monomer repeats are required in the unit cell along the *c*-axis. Note that the limited backbone coplanarity is consistent with the relatively large band gap (ca. 3 eV)[2,23] for PFO to emit blue light.

Although the alkyl side chains are preferentially in the trans conformation and tend to stretch transversely to the backbone axis (cf. Figure 3b), they do not pack in

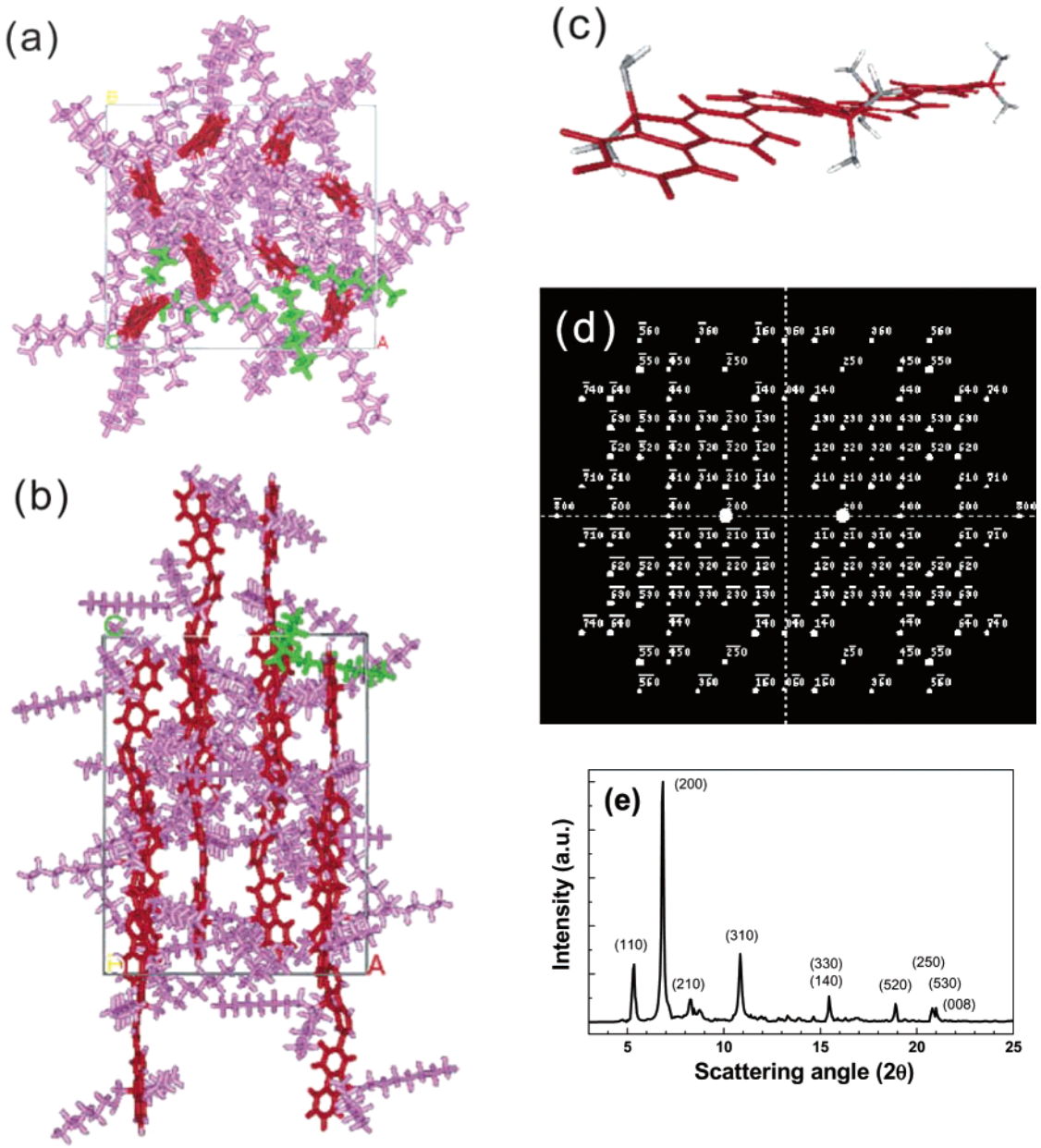

Figure 3. Proposed model of molecular packing in the crystalline phase of PF8: energy-minimized structure (backbones in red) as viewed along (a) the *c*-axis and (b) the *b*-axis; (c) an expanded view with side chains hidden to demonstrate twisting of the backbone; (d) calculated SAED [00*l*] zone pattern and (e) calculated XRD powder profile (assuming 80 × 80 × 40 nm in crystallite size, with cutoff intensity of 7.5%). A few selected pairs of *n*-octyl side chains are highlighted in green in (a) and (b) to allow for easier identification.

a particularly ordered manner as viewed along the *c*-axis (Figure 3a). Each pair of the alkyl side chains from a given monomer unit embraces a neighboring PFO backbone and serve to keep the backbones from direct close contact (the center-to-center interbackbone distance generally exceeds 0.6 nm) between parallel arrays of fluorene segments. This is consistent with the observation that crystalline PFO emission is dominated mainly by single-chromophore excitons;[13−18] earlier attributions to interchain species such as excited-state complexes (excimers) have been limited to the case of solvent-induced β-phase[16−18] or films quenched from the nematic state.[24]

Discussion

On the basis of the shadow width (cf. parts a and b of Figure 1) of a large number of single crystals, the thickness of PFO single crystals observed is estimated to be 30 nm. (The shadow width yielded thickness values mostly in the range of 15−25 nm, depending on temperature and time of crystallization.) The use of a higher estimate is to compensate for the possible underestimation as these single crystals generally sit on a matrix and could be partially buried. Attempts to obtain "clean" single crystals using thinner films failed to give single-crystal lamellae; instead, as indicated by BFI micrographs in Figure 4, nanocrystalline domains (ca. 10 nm in size) arrayed into rodlike features were observed. Similar features have been reported[25,26] for crystalline polyfluorene thin films via near-field scanning optical microscopy (NSOM), in which the conjugated backbone is shown to align transversely to the rod's long axis. Our preliminary small-angle X-ray scattering (SAXS) results on thick PFO specimens crystallized for 6 h at a lower

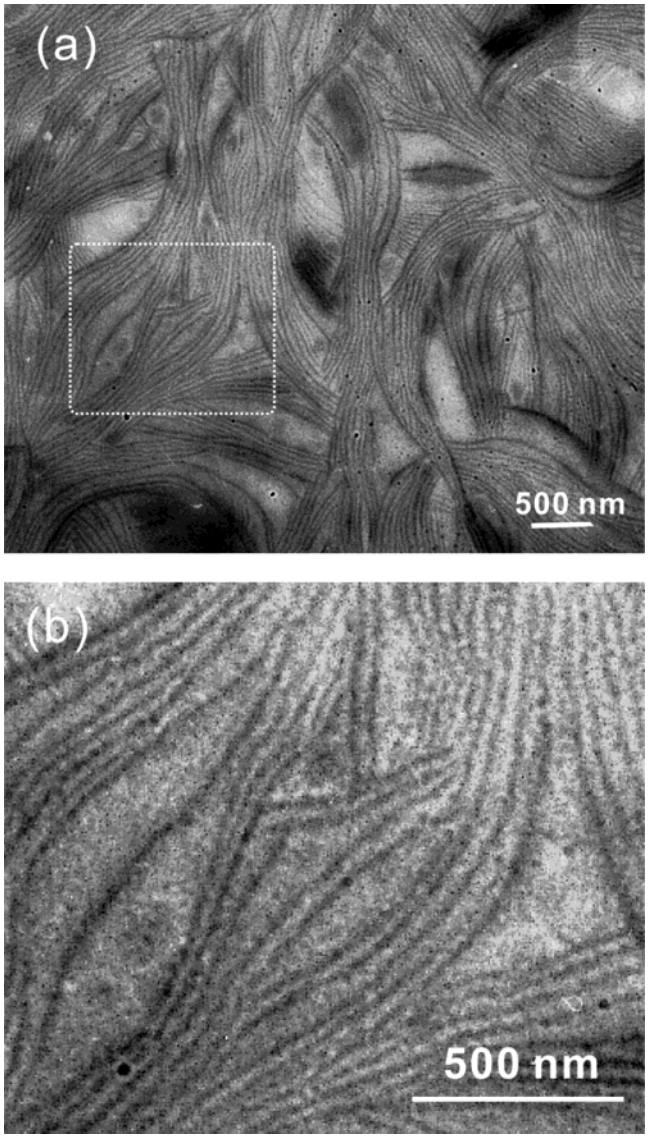

Figure 4. Representative bright field images for thin PFO specimens melt-crystallized at 135 °C for 12 h before quenching into ice water, showing (a) stringlike features that correspond to arrays of nanobeads ca. 10 nm in size as shown more clearly in (b), the blow-up view of the framed region in (a).

temperature of 130 °C (to reach sufficient crystallinity for adequate SAXS contrast) indicated a long period of ca. 10 nm, with crystalline layer thickness of ca. 4 nm (i.e., ca. 40% in crystallinity), suggesting that our estimated thickness of 30 nm (which corresponds to ca. 36 monomer units) for the PFO single crystals is indeed reasonable.

Upon correction of the PS-calibrated molecular mass values by a factor of $(2.7)^{-1}$ (as determined by Grell et al.[13] via light-scattering measurements), chain lengths of the present PFO sample correspond to a weight-average degree of polymerization $X_w = 63$ and its number-average counterpart $X_n = 24$. An assumption that only the shorter chains are responsible for formation of single crystals would allow for packing of fully extended PFO chains in the single crystals and avoid the need for chain folding. However, with this assumption, it is difficult to explain the predominant presence of nanocrystalline domains of ca. 10 nm (which corresponds to only 12 monomer repeats) in size in Figure 4.

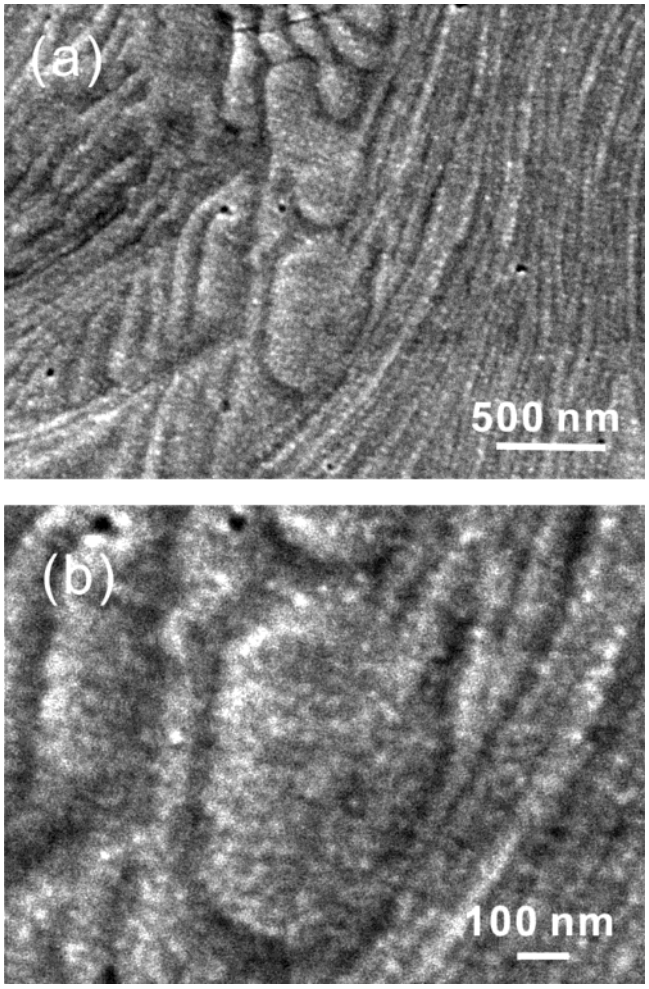

Figure 5. (a) Representative SEI of specimens crystallized at 145 °C for 12 h before quenching to 0 °C. Several single crystals, submicron in size, may be observed in the central region. Note also the stringlike features on the right-hand side and stacks of slender lamellae (or "ribbons") on the left. (b) Blow-up view showing the presence of "nanograins" in all three topographic regions.

We would like to point out further that the "nanograins" features are not limited to thin films and are quite generally observed in various crystallization conditions of PFO. Given in Figure 5 are representative SEI images showing surface topography of crystalline PFO, in which regions of stringlike features, stacks of slender crystals (or "ribbons"), and submicron single crystals may be identified. Note the presence of nanometer-scaled grainy features in all three topographic regions. In fact, nanodomains are quite generally observed in other conjugated polymers under a variety of circumstances. Examples include our earlier reports on MEH-PPV and its homologues of different side-chain structures.[5−7] Recent spectroscopic evidence[27] also indicated highly aligned intramolecular geometries in isolated MEH-PPV chains deposited on glass surface.

In view of the small size involved, these "nanobeads" or "nanograins" must be composed of essentially single (or at most a few) chains, indicating general lack of interchain entanglements during its formation. Monte Carlo simulations on conformation of collapsed semirigid chains in general[28] or MEH-PPV with tetrahedral defects in particular[29] have indicated a variety of possible morphological features ranging from toroids, bundles, to defective bundles. We consider these latter

features highly relevant to the nanograin morphology, as previously proposed by Mehta et al.[27] in their single-molecule spectroscopic study. One may envision the collapse of the isolated semirigid chains upon increase in polymer concentration (yet still below the overlap threshold) due to the rodlike nature, which encourages phase separation at a very low concentration according to Flory's classical nematic polymer solution theory.[30]

Certain form of folds must therefore be present. It is generally accepted that chemical defects do exist in conjugated polymers;[13,31,32] the chemical defects are therefore the most likely sites for folding to occur.[27,29] Effects of chemical defects are well demonstrated in chain conformation of conjugated polymers in the solution state. Reported persistent lengths (determined via small-angle scattering) of conjugated polymers in dilute solutions ranged from 2.8 nm (which translates to ca. 7 repeating units) for alkylated poly(thiophene), 8.5 nm (ca. 10 monomer units) for PFO,[13] to 15 nm (ca. 27 phenylene ethynylene repeats) for an alkylated poly(phenyleneethynylene).[33] The increasing trend with increasing backbone collinearity implies additional contributions from inherent rotational freedom. It should be emphasized here that the presumed folds in the present case of nanograins, however, are unlikely to be tight (as in classical examples of folds in polyethylene single crystals) but rather loopike, as demonstrated by results of Monte Carlo simulations.[27−29]

On the basis of the nanograin picture given above, the development of the submicron-sized PFO single crystals is unlikely to follow the classical (regime I) picture of stem-by-stem folding on the crystal front, but rather to occur first within each single nanograins. This is supported by the vast number of thin nanocrystals on top of the sub-microsized single crystals in Figure 1a,b; coalescence (presumably through micro-Brownian motion[34,35]) and thickening at the elevated temperature of crystallization of these nanocrystals should then follow, as indicated by irregularities in shape, presence of necks, and differences in shadow width (i.e., thickness) for these thin nanocrystals.

As a final remark, we add that folding of conjugated chains in the crystalline state has also been suggested[36] recently for σ-conjugated poly(di-*n*-butylsilane), although no comments on the fold structure were made. Details of the presently suggested mechanism of folding around chemical defects await further experimental clarification.

Acknowledgment. Thanks are due to Professor R. M. Ho of National Tsing Hua University, who kindly showed us techniques of preparing single crystals of semicrystalline polymers from the melt state. Thanks are also due to our colleagues at Department of Chemistry at NSYSU, including Professor C. L. Chen and Ms. S. C. Yang, for their assistance in the use of Cerius2 and Professor Y. N. Chiang for helpful discussion on crystal symmetry. We gratefully acknowledge financial support from the Ministry of Education and the National Science Council under Contracts 91E-FA04-2-4A and NSC92-2216-E-110-009, respectively.

References and Notes

(1) Kraft, A.; Grimsdale, A. C.; Holmes, A. B. *Angew. Chem., Int. Ed.* **1998**, *37*, 402.
(2) Neher, D. *Macromol. Rapid Commun.* **2001**, *22*, 1365.
(3) Scherf, U.; List, E. J. W. *Adv. Mater.* **2002**, *14*, 477.
(4) Chen, S. H.; Su, A. C.; Huang, Y. F.; Su, C. H.; Peng, G. Y.; Chen, S. A. *Macromolecules* **2002**, *35*, 4229.
(5) Chen, S. H.; Su, A. C.; Chou, H. L.; Peng, K. Y.; Chen, S. A. *Macromolecules* **2004**, *37*, 167.
(6) Chen, S. H.; Su, A. C.; Han, S. R.; Chen, S. A.; Lee, Y. Z. *Macromolecules* **2004**, *37*, 181.
(7) Chen, S. H.; Su, C. H.; Su, A. C.; Chen, S. A. *J. Phys. Chem. B* **2004**, *108*, 8855.
(8) Grell, M.; Bradley, D. D. C.; Inbasekaran, Woo, E. P. *Adv. Mater.* **1997**, *9*, 798.
(9) Teetsov, J.; Fox, M. A. *J. Mater. Chem.* **1999**, *9*, 2117.
(10) Blondin, P.; Bouchard, J.; Beaupre, S.; Belletete, M.; Durocher, G.; Leclerc, M. *Macromolecules* **2000**, *33*, 5874.
(11) Kawana, S.; Durrell, M.; Lu, J.; Macdonald, J. E.; Grell, M.; Bradley, D. D. C.; Jukes, P. C.; Jones, R. A. L.; Bennett, S. L. *Polymer* **2002**, *43*, 1907.
(12) Chen, S. H.; Su, C. H.; Su, A. C.; Chen, S. A. Manuscript in preparation.
(13) Grell, M.; Bradley, D. D. C.; Long, X.; Chamberlain, T.; Inbasekaran, M.; Woo, E. P.; Soliman, M. *Acta Polym.* **1998**, *49*, 439.
(14) Grell, M.; Bradley, D. D. C.; Ungar, G.; Hill, J.; Whitehead, K. S. *Macromolecules* **1999**, *32*, 5810.
(15) Herz, L. M.; Phillips, R. T. *Phys. Rev. B* **2000**, *61*, 13691.
(16) Cadby, A. J.; Lane, P. A.; Mellor, H.; Martin, S. J.; Grell, M.; Giebeler, C.; Bradley, D. D. C.; Wohlgenannt, M.; An, C.; Vardeny, Z. V. *Phys. Rev. B* **2000**, *62*, 15604.
(17) Winokur, M. J.; Slinker, J.; Huber, D. L. *Phys. Rev. B* **2003**, *67*, 184106.
(18) Khan, A. L. T.; Banach, M. J.; Köhler, A. *Synth. Met.* **2003**, *139*, 905.
(19) Lotz, B.; Lovinger, A. J.; Cais, R. E. *Macromolecules* **1988**, *21*, 2375.
(20) Bu, Z.; Yoon, Y.; Ho, R. M.; Zhou, W.; Jangchud, I.; Ebby, R. K.; Cheng, S. Z. D.; Hsieh, E. T.; Johnson, T. W.; Geerts, R. G.; Palackal, S. J.; Hawley, G. R.; Welch, M. B. *Macromolecules* **1996**, *29*, 6575.
(21) Ho, R. M.; Lin, C. P.; Hseih, P. Y.; Chung, T. M.; Tsai, H. Y. *Macromolecules* **2001**, *34*, 6727.
(22) Rappe, A. K.; Casewit, C. J.; Colwell, K. S.; Goddard, III, W. A.; Skiff, W. M. *J. Am. Chem. Soc.* **1992**, *114*, 10024.
(23) Janietz, S.; Bradley, D. D. C.; Grell, M.; Giebeler, C.; Inbasekaran, M.; Woo, E. P. *Appl. Phys. Lett.* **1998**, *73*, 2453.
(24) Zeng, G.; Yu, W. L.; Chua, S. J.; Huang, W. *Macromolecules* **2002**, *35*, 6907.
(25) Teetsov, J. A.; Vanden Bout, D. A. *J. Am. Chem. Soc.* **2001**, *123*, 3605.
(26) Teetsov, J.; Vanden Bout, D. A. *Langmuir* **2002**, *18*, 897.
(27) Mehta, A.; Kumar, P.; Dadmum, M. D.; Zheng, J.; Dickson, R. M.; Thundat, T.; Sumpter, B. G.; Barnes, M. D. *Nano Lett.* **2003**, *3*, 603.
(28) Noguchi, H.; Yoshikawa, K. *J. Chem. Phys.* **1998**, *109*, 5070.
(29) Hu, D.; Yu, J.; Wong, K.; Bagchi, B.; Rossky, P. J.; Barbara, P. F. *Nature (London)* **2000**, *405*, 1030.
(30) Flory, P. J. *Proc. R. Soc. London* **1956**, *A234*, 73.
(31) Yan, M.; Rothberg, L. J.; Papadimitrakopoulos, F.; Galvin, M. E.; Miller, T. M. *Phys. Rev. Lett.* **1994**, *73*, 744.
(32) Inigo, A. R.; Chiu, H. C.; Fann, W.; Ying-Sheng Huang, Y. S.; Jeng, U. S.; Hsu, C. H.; Peng, K. Y.; Chen, S. A. *Synth. Met.* **2003**, *139*, 581.
(33) Cotts, P. M.; Swager, T. M.; Zhou, Q. *Macromolecules* **1996**, *29*, 7323.
(34) Métois, J. J.; Gauch, M.; Masson, A.; Kern, R. *Surf. Sci.* **1972**, *30*, 43.
(35) Kuo, L. Y.; Shen, P. *Surf. Sci.* **1997**, *373*, L350.
(36) Hu, Z.; Zhang, F.; Huang, H.; Zhang, M.; He, T. *Macromolecules* **2004**, *37*, 3310.

MA049346A